LIGO-P070044-00-Z

Effects of mode degeneracy in the LIGO Livingston Observatory recycling cavity

Erika D'Ambrosio*
LIGO Laboratory, California Institute of Technology, MS 18-34, Pasadena, CA 91125, USA

Andri M. Gretarsson†
Embry-Riddle Aeronautical University, 3700 Willow Creek Rd., Prescott, AZ 86301, USA.

Valery Frolov and Brian O'Reilly
LIGO Livingston Observatory, Livingston LA 70754, USA.

Peter K. Fritschel
LIGO Project, Massachusetts Institute of Technology, NW17-161, 175 Albany Street, Cambridge, MA 02139, USA

We analyze the electromagnetic fields in a Pound-Drever-Hall locked, optically unstable, Fabry-Perot cavity as a function of small changes in the cavity length during resonance. More specifically, our investigations focus on the recycling cavity of the Laser Interferometer Gravitational-wave Observatory (LIGO) detector that is located in Livingston, Louisiana. In the interferometer's normal mode of operation, the recycling cavity is stabilized by inducing a thermal lens in the cavity mirrors using an external CO_2 laser. During the study described here, this thermal compensation system was not operating, causing the cavity to be marginally optically unstable and cavity modes to become degenerate. In contrast to stable optical cavities, the modal content of the resonating beam in the uncompensated recycling cavity is significantly altered by very small cavity length changes. The separation of the longitudinal and transverse degrees of freedom is destroyed and the standard Hermite-Gauss labeling, that applies to stable cavity modes, loses its utility. The optical instability modifies the error signals used to control the cavity length in such a way that the zero crossing point is no longer the point of maximum power in the cavity nor is it the point where the input beam mode in the cavity is maximized.

I. INTRODUCTION

The LIGO [1–3] recycling cavity was designed to be optically stable at full input power which implies thermally induced lensing of the recycling cavity optics during full power operation [4, 5]. This article presents measurements of the fields in the recycling cavity when the input power is set low enough so that no significant thermal lensing occurs due to absorption of the resonating beam in the cavity optics. In this state, the recycling cavity is optically unstable in the sense that it is not mode selective. ($g_1 g_2 \approx 1.0003$, ignoring beamsplitter curvature which should not have a large common mode effect.) Therefore, the recycling cavity beam is not matched to the fundamental optical mode of interferometer arms, nor to the input beam which is designed to closely match the fundamental mode of the arms. Optical fields, such as the sideband fields, that resonate in the recycling cavity but do not resonate in the arms, exhibit a ringlike structure; and small angle or length perturbations of the cavity have a significant effect on the features of these fields. This chaotic response is due to the non separability of the boundary conditions on the optical fields leading to mode degeneracy. Due to this behaviour, and the large number of modes involved, it is no longer efficient to express the cavity field in terms of the usual Hermite-Gaussian (or Laguerre-Gaussian) modes. [6]. We therefore chose to use a numerical simulation based on the Fast Fourier Transform, rather than on the propagation of a large number of cavity modes. This simulation software is referred to as "The FFT Model". [7] As a result of the sensitivity of the transverse field distribution to small length changes, we find that the Pound-Drever-Hall error signal [8] used to control the length of the cavity is modified and the lock-point develops an unexpected offset.

We tested the model against actual interferometer behavior by applying a series of offsets to the error point of the length loop of the recycling cavity of the Livingston interferometer. [9] (The length loop in question is the common mode length loop which acts on the position of the recycling mirror.) We recorded the power in the cavity for a range of offsets and also acquired images of the light distribution inside the cavity and on reflection from the cavity. We then compared our results to those of the simulation. Although the FFT Program has previously been used to

* ambrosio_e@ligo.caltech.edu
† greta9a1@erau.edu

gain insight into power build-up effects of the LIGO interferometers [10], this study is unusual in that it provides a direct, well controlled, quantitative comparison between the predictions of the model and the observed interferometer behavior.

II. MEASUREMENT OVERVIEW

To make the optical fields easier to model, and to make the interpretation of the results simpler, most of our measurements were taken when the arms were unlocked and the recycling cavity was locked so that the carrier was resonant in the recycling cavity while the the sidebands were non-resonant. By adding an offest to the error point of the Pound-Drever-Hall locking servo controlling the length loop of the recycling cavity, we induced small length changes of the cavity with respect to the null point of the servo. We could change the cavity length by several nanometers before lock was lost. The length offset was calibrated in terms of actual cavity length change in nanometers which allowed a quantitative comparison between our simulation results and the experimental data. A description of the calibration procedure is available in the form of an excerpt from the interferometer detector log [11]. We obtained the cavity power as a function of the length offset and obtained images of the cavity beam profile at various offsets. We also made preliminary measurements with the full interferometer locked. (In the fully locked state the carrier is resonant in all optical cavities and the sidebands are simultaneously resonant, but only in the recycling cavity.) No attempt was made to model the fields in the fully locked interferometer.

The schematic diagram in Fig. 3 illustrates the general configuration. To obtain information about the intensity distribution of the fields interacting with the cavity, we used two CCD cameras: One captured the light reflected from the cavity and the other captured light picked out of the cavity by means of the slightly wedged antireflective side of one of the mirrors. To measure the power in the cavity, we used a calibrated photodiode, operating at DC, monitoring the intensity of the beam picked off at the slightly wedged antireflective side of the beamsplitter. The beam picked off at the antireflective side of the beamsplitter, like the beam picked off at the antireflective side of the arm input test masses, is a good representation of the recycling cavity beam.

In the case of the fully locked interferometer, we used different methods to provide information about the sidebands in the recycling cavity. When the full interferometer is locked, the recycling cavity field intensity is dominated by the carrier so we could not use a DC coupled photodiode or a CCD camera for our purpose of interrogating the RF sidebands. To measure the intensity of the sidebands, we used an RF photodiode whose signal was demodulated at twice the sideband frequency. This photodiode received a highly focused version of the beam picked off from the antireflective side of the beamsplitter. The signal from this photodiode is proportional to the geometric mean of the power in the upper and lower sidebands. We employed a similar technique to measure the spatial profile of the sideband intensity using a "phase camera" [12]. The phase camera rapidly scans an enlarged version of the beam sampled from the recycling cavity over an RF photodiode which is very small compared to the size of the beam. This allowed us to reconstruct the spatial profile of the geometric mean of the upper and lower sideband intensities. The phase camera received the recycling cavity beam picked off from the slightly wedged antireflective side of ITMY.

III. FFT MODEL OVERVIEW

The numerical simulation with which we compare our measurements—The FFT Model [7]—is based on a Fortran script whose first step is a Fourier transformation of the grid representation of the optical field. In the wave vector domain, a matrix multiplication provides the propagation of the field; then, when the interaction with the optics must be reproduced, the optical field is Fourier transformed back from the momentum representation to the spatial one and each element of the grid is multiplied by a phase delay that describes the action of the optics. Once iterative propagation has terminated and the resulting fields are stationary, we construct the the Pound-Drever-Hall error signal from the fields.

IV. RESULTS

A. Carrier resonant in the recycling cavity, arms non-resonant

Figure 1 compares the resonant field intensity derived from the FFT model with the actual measured field intensity as a function of cavity length. The intensity distribution changes dramatically with small changes of the cavity length. Note that the FFT model correctly reproduces the evolution of the beam shape as it goes from a one-peak profile to a donut and also reproduces the relative increase in beam size.

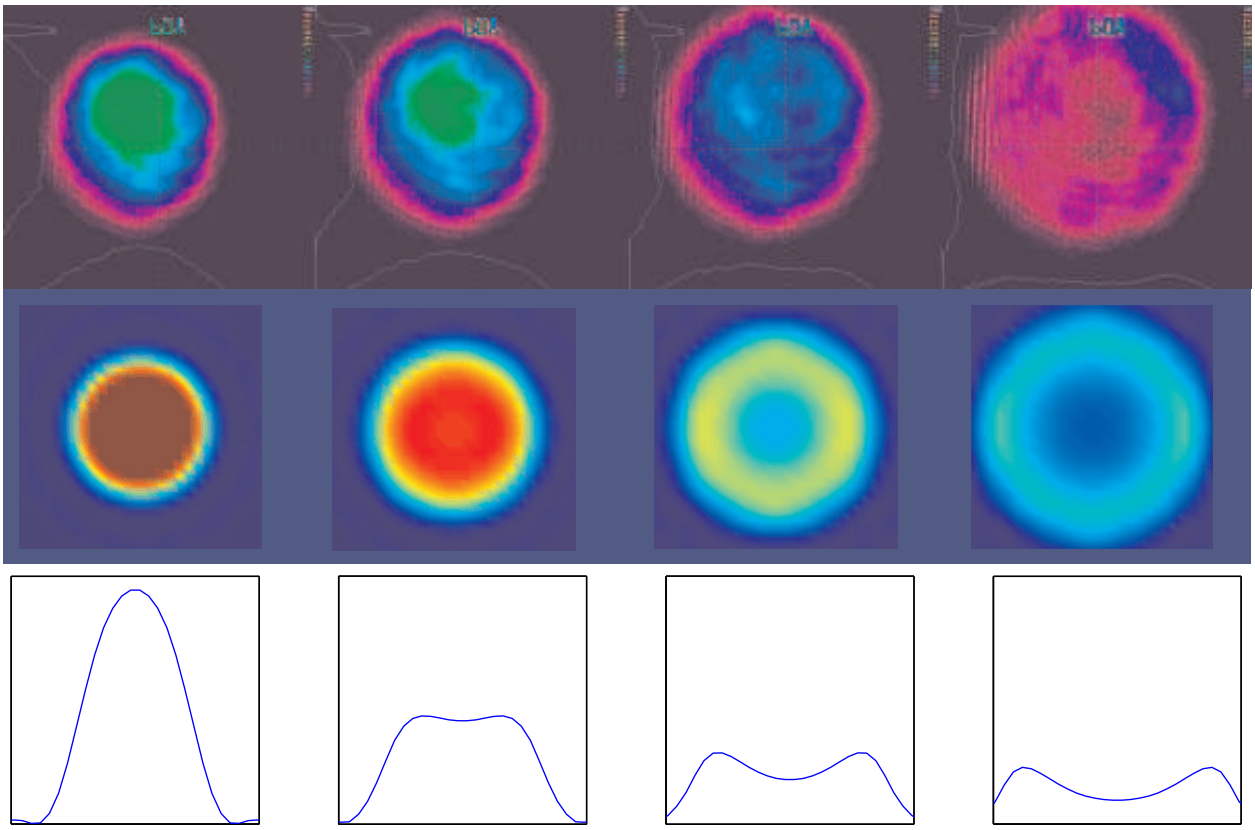

FIG. 1: Effect of changing the cavity length by several nanometers on the shape of the carrier resonating in the recycling cavity. Arms are not resonant. Comparison of actual image captures with model predictions. The top row shows a false color image of the intensity of the recycling cavity beam picked off at ITMY. The colors represent intensity (magenta is minimum while green is maximum). The central and bottom row shows the FFT model results for the same cavity length offsets. (Dark-blue represents minimum intensity while dark red represents maximum intensity.) From left to right, for both simulation results and experimental observations, the offsets are: **-8nm**, **-4nm**, **0nm**, and **+4nm**. For reference, the diameter of the ring structure in the rightmost image in the central row is 5 cm. The units of distance represented by the axes are left arbitrary because the actual physical dimensions of images rendered by camera were not known. (In other words, a camera calibration was not available.)

Figure 2 compares the measured cavity power with the prediction from the FFT model. The point of maximum power found by the FFT model agrees with the measurement as does the approximate power build-up. The fact that the power data fall generally below the prediction for the larger length offsets is related to a loop gain reduction which produces a change in the calibration. This causes an underestimation of the cavity length variation for those offsets that are quite far from the point of maximum cavity power. The figure also shows the portion of the power in the TEM_{00} mode, which is the mode of the input beam to the recycling cavity (fundamental mode of the modecleaner propagated through the mode-matching telescope towards the interferometer). By design, the input beam mode is closely mathced to the TEM_{00} mode of the 4 km arm cavities. Unexpectedly, and in contrast to the behavior seen in optically stable cavities (even ones whose input beams are not matched to the cavity mode) the FFT model shows that the power in the TEM_{00} component is maximized even further from the locking point than the total cavity power.

To gain insight into this unusual behavior, we write down a general expression the Pound-Drever-Hall error signal that makes no assumptions about the spatial profile of the beams involved. The notation refers to the fields indicated in Fig. 3.

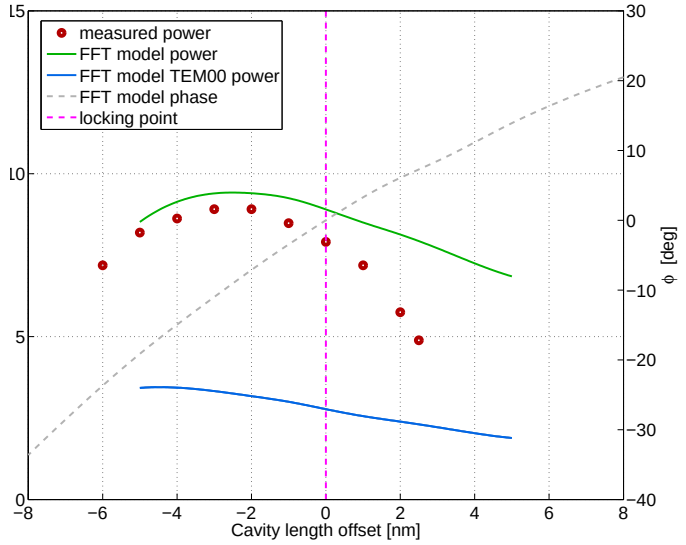

FIG. 2: Power in the recycling cavity as a function of cavity length offset. The FFT Model accurately predicts the length offset at which the cavity power is maximized. The green line shows the FFT model prediction for the total cavity power. The blue line shows the FFT model prediction for the power in the mode of the input beam to the cavity. The scale on the right refers to the dashed line representing the FFT model phase $\phi = \mathrm{Arg}\left(\langle \Psi_{\mathrm{LASER}} | \Psi^{CR}_{REFL} \rangle\right)$ in the notation below, which is set to zero at the locking point.

The Pound-Drever-Hall error signal is generated by phase modulating the input beam to the cavity

$$\begin{aligned} \Psi_{IN} &= \Psi_{\mathrm{LASER}} \exp[i\Gamma \cos\omega t] \\ &\simeq J_0(\Gamma)\,\Psi_{\mathrm{LASER}} + iJ_1(\Gamma)\,\Psi_{\mathrm{LASER}} \exp[i\omega t] + iJ_1(\Gamma)\,\Psi_{\mathrm{LASER}} \exp[-i\omega t] + \ldots \\ &\equiv \Psi^{CR}_{IN} + \Psi^{SB+}_{\mathrm{IN}} \exp[i\omega t] + \Psi^{SB-}_{\mathrm{IN}} \exp[-i\omega t] + \ldots \end{aligned} \tag{1}$$

where ω is the modulation frequency and Γ is the modulation depth. The input field is therefore often considered as three collinear beams: the carrier, Ψ^{CR}_{IN}, and a pair of sidebands, Ψ^{SB+}_{IN} and Ψ^{SB-}_{IN}, with frequency separation ω on either side of the carrier frequency. The 24.5 MHz modulation frequency is such that when the carrier beam is resonant in the recycling cavity, the sidebands are nearly anti-resonant and thus nearly totally reflected from the input mirror (the recycling mirror). In these circumstances, only the carrier is significantly sensitive to the geometrical features of the cavity, including length variations or alignment, as described by the equations

$$\begin{aligned} \Psi^{SB-}_{\mathrm{REFL}} &\simeq -\Psi^{SB-}_{\mathrm{IN}} \\ \Psi^{SB+}_{\mathrm{REFL}} &\simeq -\Psi^{SB+}_{\mathrm{IN}} \\ \Psi^{CR}_{REFL} &= D\Psi^{CR}_{IN} \end{aligned} \tag{2}$$

where D includes any effect of the cavity on the resonant carrier. The total reflected power is the integral of the squared field, corresponding to the sum of the three returning fields

$$\begin{aligned} P_{\mathrm{REFL}} &= \int_S |\Psi_{\mathrm{REFL}}|^2\, dS = \int_S \left\{ |\Psi^{CR}_{\mathrm{REFL}}|^2 + |\Psi^{SB+}_{\mathrm{REFL}}|^2 + |\Psi^{SB-}_{\mathrm{REFL}}|^2 \right. \\ &\quad + 2\Re\left[(\Psi^{CR}_{\mathrm{REFL}} {\Psi^{SB-}_{\mathrm{REFL}}}^* + \Psi^{SB+}_{\mathrm{REFL}} {\Psi^{CR}_{\mathrm{REFL}}}^*) \exp(i\omega t) \right] \\ &\quad \left. + 2\Re\left[\Psi^{SB+}_{\mathrm{REFL}} {\Psi^{SB-}_{\mathrm{REFL}}}^* \exp(2i\omega t) \right] + \ldots \right\} dS \end{aligned} \tag{3}$$

where S is always an area of integration much larger than the beam size. To lock the cavity, we need to control both the common mode length of the cavity (average of the two paths of the cavity) and the differential one [15]. We are

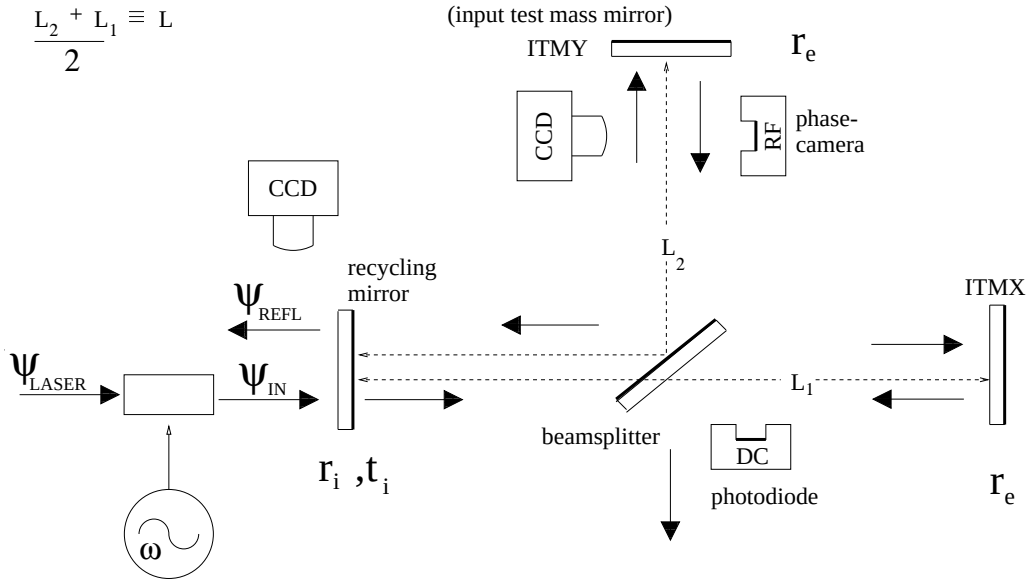

FIG. 3: The laser field $\Psi_{\rm LASER}$ is phase modulated to produce $\Psi_{\rm IN}$ consisting of approximately 90% carrier light and 5% each upper and lower phase modulation sidebands, 24.5 MHz on each side of the carrier. The reflected field $\Psi_{\rm REFL}$ is the sum of three components: the sidebands, which are almost completely reflected back towards the laser since the cavity length makes them non resonant, the prompt reflection of the carrier that is not interacting with the recycling cavity, and the loss through the recycling mirror of the carrier field resonating inside the cavity. The cavity beam is split by the beam splitter into two paths of different lengths, represented in the diagram by L_1 and L_2. The amplitude transmission and reflection coefficients are represented by t_i and r_i respectively. The position of the beam splitter is actively controlled, so that its antisymmetric port corresponds to the dark fringe of the carrier.

interested in the common length of the cavity only, whose error signal is the same as the error signal from a simple two-mirror cavity. This signal is V_I, the I-phase of the demodulated voltage from an RF photodiode placed at the reflected port where $P_{\rm REFL}$ is sensed. Using the same modulation frequency ω for demodulation, one term survives

$$\begin{aligned} V_I &\approx \alpha \int_S dS \int_0^T dt \, \frac{P_{\rm REFL}\cos(\omega t)}{T} \\ &= \alpha \int_S \Re(\Psi^{CR}_{\rm REFL}\Psi^{SB-\,*}_{\rm REFL} + \Psi^{SB+}_{\rm REFL}\Psi^{CR\,*}_{\rm REFL})\, dS \end{aligned} \tag{4}$$

where $\Re$ indicates the real part, $T \gg \omega^{-1}$ is the effective integration time of the sensing chain and α is an overall (real) constant which represents the efficiency of the photodetection. Rewriting the integrals as inner products brings out the structure—

$$\begin{aligned} V_I &\propto \Re\left[\,\langle\Psi^{CR}_{\rm REFL}|\Psi^{SB-}_{\rm REFL}\rangle + \langle\Psi^{SB+}_{\rm REFL}|\Psi^{CR}_{\rm REFL}\rangle\,\right] \\ &= 2J_1(\Gamma)\,\Im\,\langle\Psi_{\rm LASER}|\Psi^{CR}_{REFL}\rangle\,. \end{aligned} \tag{5}$$

Equation (5) makes it obvious that the error signal is generated only from the component of the returning carrier that is in the mode of the input beam. Therefore, for *stable* cavities, where different modes are separated by a discrete Gouy phase, the Pound-Drever-Hall locking technique selects the length of the cavity so that the eigenmode of the cavity field having greatest overlap with the mode of the input beam is resonant. When a low-loss eigenmode of the cavity is well matched to that of the input beam, large buildups of that cavity mode occur. The imaginary part of the overlap integral in Eq. (5) becomes zero when the phase of the input beam mode component of the returning carrier matches the phase of the input beam . This corresponds to maximizing the power of the input beam mode component of the cavity field.

For non-separable boundary conditions, the eigenmode decomposition breaks down and the transverse shape of the cavity beam depends strongly on the cavity length. The Pound-Drever-Hall error signal is modified by this spatial dependence in such a way that minimization of the error signal is no longer equivalent to maximizing the cavity field in the mode of the input beam. In other words, the natural lock-point of the servo is no longer the point at which the

power in the input beam component of the cavity field is maximized. (The total cavity power is also not maximized at the natural lock point but that is not unexpected.) From the naive point of view therefore the servo has developed an offset. Physically, this offset appears to be due to a competition between the cavity length change and spatial beam profile change for efficiently coupling light into the cavity.

The high level of agreement between the experimental observations and the FFT optical model, indicate that the observed loop offset is a true optical effect, and is not due to a simple technical effect such as unintended offsets in the control electronics. Such an offset can therefore be expected to develop in other marginally unstable cavities locked by the Pound-Drever-Hall technique. Resonant points of such cavities may need to be adjusted "by hand" to compensate. In particular, we note that qualitatively similar behavior has been observed at LIGO Hanford Observatory. [14] The maximum power built up in the recycling cavity at LIGO Hanford Observatory also occurs only when an offset is applied to the natural lock point and transverse beam profile changes are evident as well.

B. Full interferometer lock

When the full interferometer is locked, the intensity in the recycling cavity is dominated by the carrier whose spatial structure is set by the input conditions to the arm to be the TEM_{00} mode of the optically stable arm cavities (which is closely matched by input beam to the interferometer). When the full interferometer is locked, the TEM_{00} mode of the arm cavity has the correct frequency and transverse shape to allow it to resonate in both the recycling cavity and the arms. The sidebands on the other hand, being non-resonant in the arms, experience *almost* the same conditions as the carrier when the carrier is resonant in the recycling cavity with the arms non-resonant. Therefore, we can expect the field structure of the sidebands in the full lock to be qualitatively similar to the carrier field distribution of Section IV A. Phase camera images of the sideband intensity taken from the beam picked off at the antirefltective side of ITMY are shown in Figure 4. The colors in this image indicate the geometric mean of the intensity of the two sidebands. For technical reasons, we did not obtain a calibration of the offset in terms of length.

Figure 5 shows the (geometric mean of the) power of the sidebands in the recycling cavity as the cavity length is changed. The x-axis shows the offset added to the error point in uncalibrated counts. The y-axis is the mean of the interferometer NSPOB channel representing the geometric mean of the upper and lower sideband powers. Note that we see a much larger change in the sideband intensity in this fully locked state than the change in the carrier intensity for the carrier lock in the recycling cavity. The reason for this is most probably that as the profile of the sidebands in the recycling cavity begins to better match the resonating mode of the arm cavities, a larger fraction of the beam is exactly on antiresonance and is totally reflected from the arm thus enhancing the build up of the sidebands in the recycling cavity. As expected, the qualitative behavior of the sideband power and transverse profile is the same as that of the carrier in Section IV A. The shape of the cavity beam changes as a function of length and the lock point does not correspond to maximum sideband power in the cavity. Although we could not extract the TEM_{00} component of the sidebands from the intensity alone, it seems likely based on the analysis of Section IV A that it is also not maximized.

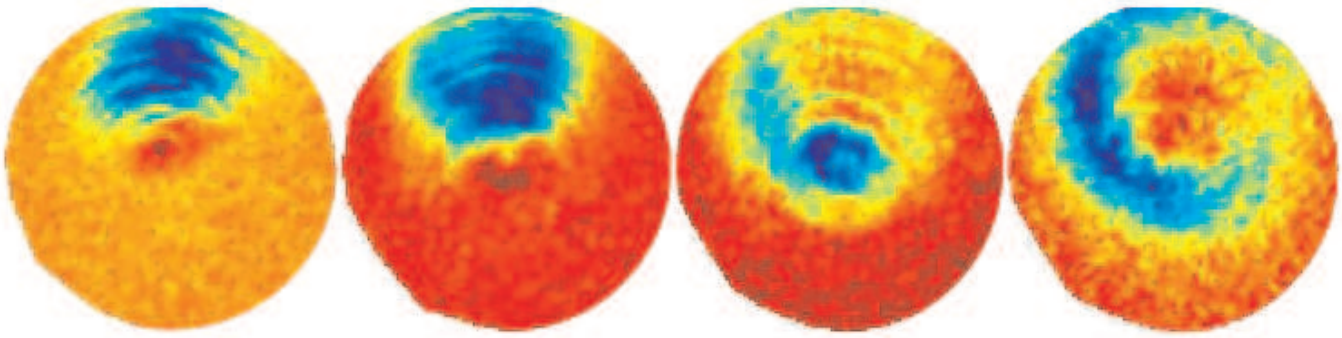

FIG. 4: Effect of changing the cavity length by several nanometers on the shape of the sidebands resonating in the recycling cavity. The colors represent the geometric mean of the intensity of the upper and lower sidebands. (Note that in these images, the center of the beam is in the upper half of the image.) The third image from the left represents the natural lock point (zero applied offset). The non-symmetrical structure of some images is largely due to pitch motion of the optics affecting the instantaneous field distribution.

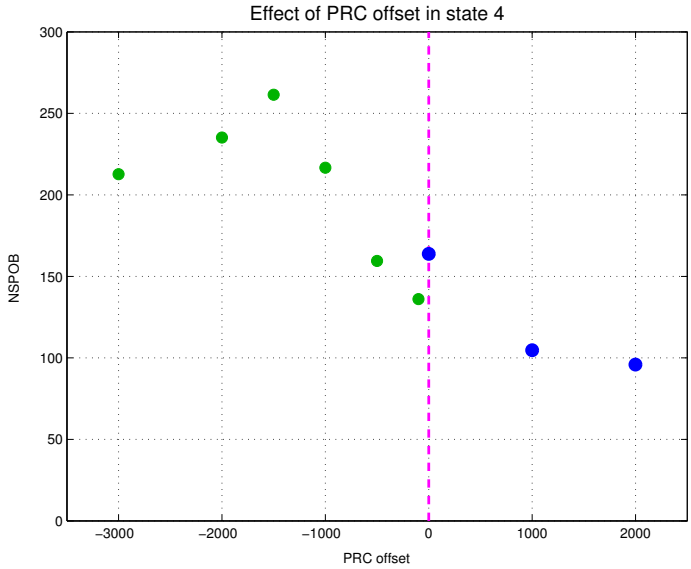

FIG. 5: Sideband intensity as a function of uncalibrated length offset. This graph contains data from two lock stretches which we have distinguished by the green and blue colors.

Acknowledgements

The continuing and reliable operation of the LIGO interferometer at Livingston is made possible by the hard work of our many commissioning colleagues. The authors thank them and the LIGO Scientific Collaboration for the use of the instrument. Rana Adhikari taught one of the authors [AMG] how to understand the LIGO Livingston interferometer and also provided useful comments for the paper. David Ottaway read versions of the manuscript and shared insights based on his considerable knowledge of the interferometer optics. He was also one of the first people to appreciate the importance of the non-gaussian structure of the sidebands in the LLO recycling cavity, first seen during installation and commissioning of the LLO phase camera with one of the authors [AMG]. The authors thank Riccardo DeSalvo and David Reitze for encouraging the submission of the manuscript for publication. LIGO was constructed by the California Institute of Technology and Massachusetts Institute of Technology with funding from the National Science Foundation and operates under cooperative agreement PHY-0107417.

[1] Abbott et al., Nucl. Instr. and Methods **A517**, 154 (2004).
[2] A. Abramovici et al., Science **256**, 325 (1992).
[3] P. Fritschel, Applied Optics **40**, 4988 (2001), http://adsabs.harvard.edu/abs/2001ApOpt..40.4988F.
[4] R. Beusoleil, E. D'Ambrosio, B. Kells, J. Camp, E. Gustafson, and M. Fejer, J. Opt. Soc. Am. B **20**, 1247 (2003).
[5] B. Kells and J. Camp, http://www.ligo.caltech.edu/docs/T/T970097-01.pdf (1997).
[6] E. D'Ambrosio Physical Review D **73**, 122002 (2006) on the tensorial description of complex coupled cavities and the non-separability of transverse and longitudinal degrees of freedom in Michelson interferometers.
[7] B. Bochner, http://www.ligo.caltech.edu/docs/P/P980004 (1998), FFT Model Description.
[8] R. W. P. Drever et al., Applied Physics B **31**, 97 (1983), for a thorough elucidation of the Pound-Drever-Hall technique.
[9] URL `www.ligo-la.caltech.edu` The measurements described were made during March, 2004.
[10] E. D'Ambrosio, Class. and Quant. Gravity **21**, 1113-1120 (2004).
[11] Andri M. Gretarsson, Valera Frolov, URL `http://www.ligo.caltech.edu/docs/T/T070074-00.pdf` (2004).
[12] K. Goda, D. Ottaway, B. Connelly, R. Adhikari, N. Mavalvala, and A. Gretarsson, Opt Lett **29**, 1452 (2004), URL `http://eutils.ncbi.nlm.nih.gov/entrez/eutils/elink.fcgi?cmd=prlinks\&dbfrom=pubmed\&retmode=ref\&id=15259710`.
[13] F. A. Jenkins and H. E. White, *Fundamentals of Optics, 4th Ed* (McGraw-Hill, 1976).
[14] *David Ottaway, Private Communication, 2005.*
[15] The differential length is sensed at the antisymmetric port using the very small amount of sideband light leaking out of the beamsplitter